Adsorption Kinetics of *n*-Nonyl-β-D-glucopyranoside at the Air−Water Interface Studied by Infrared Reflection Absorption Spectroscopy

Annette Meister, Andreas Kerth, and Alfred Blume*

Institute of Physical Chemistry, Martin Luther University Halle-Wittenberg, Mühlpforte 1, D-06108 Halle, Germany

Received: October 21, 2004; In Final Form: January 28, 2005

The adsorption of the surfactant *n*-nonyl-β-D-glucopyranoside at the air−water interface after injection of the surfactant into the subphase was studied by infrared reflection absorption spectroscopy. In the first part, we investigated the equilibrium adsorption of *n*-nonyl-β-D-glucopyranoside and the Gibbs adsorption isotherm was measured by applying the film balance technique. In the second part, the adsorption kinetics was followed by changes in the surface pressure and in the intensities of the OH band, which is related to the layer thickness, and the CH_2 antisymmetric stretching vibrational band. During an induction period, when the molecules are still highly diluted and the surface pressure is low, they are oriented parallel to the air−water interface. IR band simulations for the CH_2 antisymmetric stretching vibrational band support the idea of horizontally oriented molecules at the air−water interface. Later on, when more molecules are adsorbed to the air−water interface, they suddenly rearrange to an upright orientation as indicated by changes of the OH and the CH_2 bands. The observations are discussed in comparison to results obtained for the adsorption kinetics of *n*-decyl-β-D-maltopyranoside, *n*-dodecyl-β-D-maltopyranoside, and sodium dodecyl sulfate.

Introduction

The adsorption behavior of amphiphiles, which self-assemble at the air−water interface as Gibbs or Langmuir monolayers, is a subject of growing interest.[1−11] Kinetic,[11−13] thermodynamic,[6,14] and electric[15−17] methods have been applied to investigate the surface properties of amphiphilic molecules, and new sensitive surface spectroscopic techniques (X-ray and neutron reflectivity,[18] linear and nonlinear optical techniques,[19−21] sum-frequency spectroscopy,[22] and surface plasmon spectroscopy[23]) have been developed. Insights into the microscopic and submicroscopic structures have been provided by Brewster angle microscopy (BAM),[24] X-ray diffraction at gracing incidence (GIXD),[25] Raman scattering,[26] and infrared reflection absorption spectroscopy (IRRAS).[27]

Nevertheless, there is still a lack of understanding of the structural arrangement of amphiphiles at the air−water interface at low degree of coverage. Low surface concentrations seem to favor the formation of "surface micelles", first proposed by Langmuir in the 1930s and discussed in the literature.[28,29] Unfortunately, current techniques are not able to visualize those small aggregates, but experimental hints from optical techniques, X-ray diffraction, atomic force microscopy (AFM), and electron spin resonance (ESR) support the existence of those nanodomains.[30−33] Israelachvili[34] presented a thermodynamic description for the formation of surface micelles, their aggregation numbers, and the molecular orientation within the micelles. In contrast to the classical monolayer arrangement with acyl chains perpendicular to the surface, he proposed disk or ribbonlike micelles with a flat orientation of the amphiphiles.

Recently, the term "surface micelles" was applied to round-shaped nanometer-sized micelles of semifluorinated alkanes and fatty acids self-assembled at the air−water interface, which were investigated by GIXD, by polarization modulation (PM)-IRRAS, and after deposition by AFM.[35−37] The orientation of the molecules within these micelles is perpendicular to the water surface and differs from that of flat micelles with molecules lying parallel to the water surface.

Further support for a possible horizontal orientation of amphiphiles was given by Lunkenheimer applying surface potential and surface laser light scattering investigations.[15,38] He described the adsorption of surfactants by means of a two-state model including the transition from a flat to an upright surface orientation.[39]

The injection of water-soluble surfactants with low critical micelle concentration (cmc) and hence monomer concentration into water leads to very slow adsorption kinetics at the air−water interface. In their pioneering theoretical work on adsorption kinetics, Ward and Tordai[40] solved the problem of adsorption with a general theory of diffusion to the surface, which allows for back-diffusion. Fainerman and Miller[41] considered the effect of a nonequilibrium surface layer on the dynamic surface tension in a diffusion-controlled adsorption model. Prosser et al.[11] described dynamic surface tension measurements for *n*-dodecanoic acid, which showed a pronounced induction time together with the formation of monolayer islands.

In this paper, we focus on the adsorption kinetics of *n*-nonyl-β-D-glucopyranoside (NG) at the air−water interface studied by a combination of surface pressure measurements and IRRA spectroscopy. The behavior of NG is characterized by changes in the arrangement of NG molecules at the air−water interface, and it is compared to the adsorption kinetics of *n*-decyl-β-D-maltopyranoside (DeM), *n*-dodecyl-β-D-maltopyranoside (DodeM), and sodium dodecyl sulfate (SDS).

Materials and Methods

Chemicals. The surfactants NG (99% purity), DeM and DodeM (>99% purity), and SDS (99% purity) were purchased

* To whom correspondence should be addressed. Phone: +49-345-5525850. Fax: +49-345-5527157. E-mail: blume@chemie.uni-halle.de.

10.1021/jp045196u CCC: $30.25
Published on Web 03/05/2005

from Bachem (Bubendorf, Switzerland), Anatrace (Maumee, OH), and Sigma (Steinheim, Germany), respectively. The products were used without further purification. For the IRRAS measurements deionized water with a resistivity of 18.2 MΩ cm (SG Wasseraufbereitung und Regenerierstation GmbH, Barsbüttel, Germany) was used as subphase.

IRRAS Measurements. All experiments were performed with a Wilhelmy film balance (Riegler & Kirstein, Berlin, Germany), using a filter paper as Wilhelmy plate. Two Teflon troughs of different size (300 × 60 × 3 mm and 60 × 60 × 3 mm for the reference trough) were linked by three small water-filled bores to ensure equal height of the air−water interface in both troughs. The temperature of the subphase was maintained at 20 ± 0.5 °C. The movement of the Teflon barriers of the larger sample trough was computer-controlled. Measurements were performed in the small trough, the larger one usually serving as reference trough. A Plexiglas hood covered both troughs in order to minimize evaporation of water and to keep the humidity constant.

Infrared spectra were recorded with an Equinox 55 FT-IR spectrometer (Bruker, Karlsruhe, Germany) connected to an XA 511 reflection attachment (Bruker) with an external narrow band MCT detector. The IR beam is focused by several mirrors onto the water surface, and different angles of incidence can be adjusted. A computer-controlled rotating KRS-5 polarizer (>98% degree of polarization) was used to generate parallel and perpendicularly polarized light. The trough system was positioned on a moveable platform to be able to shuttle between the sample and the reference trough. This shuttle technique diminishes the spectral interferences due to the water vapor absorption in the light beam.[42]

The acquisition of the IRRAS spectra started directly after the injection of the surfactant into the subphase. In all experiments the angle of the incident infrared beam (s-polarized) was 40° with respect to the normal of the water surface. Spectra were recorded at a spectral resolution of 4 cm^{-1} using a Blackman−Harris four-term apodization and a zero filling factor of 2. For each spectrum 1000 scans were co-added over a total acquisition time of 1 min 20 s. The single beam reflectance spectrum of the reference trough surface was ratioed as background to the single beam reflectance spectrum of the monolayer on the sample trough to calculate the reflection absorption spectrum as $-[\log(R/R_0)]$. For the determination of wavenumber maxima from spectra corresponding to different surfactant concentrations, eight IRRA spectra from the surface pressure plateau regions were averaged in order to increase the precision to ±0.3 cm^{-1}.

Adsorption of Surfactants. Surfactant solutions were injected into the water subphase of the small IRRAS trough in small volume increments by means of a syringe to obtain the desired subphase concentrations. Just before each injection the needle was cleaned with a paper tissue, but without use of solvent. The surfactant stock solutions were 0.4 M for NG, 0.2 M for DeM, 0.04 M for DodeM, and 0.405 M for SDS. After each injection an equilibration time of up to 3 h was needed until a constant surface pressure was reached.

Additional adsorption experiments were performed with a round home-built Teflon trough with a total area of 7.07 cm^2 and a volume of 11.15 mL. Surfactant solutions were injected with a Hamilton syringe through the Teflon jacket just above the bottom of the trough. Tiny magnets stirred the subphase to ensure a homogeneous distribution of the surfactant. The surface pressure was measured by the Wilhelmy method, using a filter paper as the Wilhelmy plate. The temperature of the subphase was maintained at 20 ± 0.5 °C, and a Plexiglas hood covered the trough to minimize evaporation of water.

Calculation of Vibrational Modes. The energy optimized structure of NG was calculated using the *COMPASS* force field in the *Discover* module of *Materials Studio* (Accelrys Inc.). Then, the normal mode calculation of the energy-minimized structure of NG was performed to obtain the vibrational frequencies of the relevant groups.

Results and Discussion

Equilibrium Adsorption of NG. The adsorption of NG at the air−water interface can be followed by IRRAS, monitoring the methylene stretching modes at about 2925 and 2850 cm^{-1}, the C−O−C ring stretching and C−O−H deformational modes of the sugar headgroups (990−1079 cm^{-1}), and the OH stretching band at about 3560 cm^{-1}. The Wilhelmy plate technique allows the correlation of this structural information with the surface pressure. IRRA spectra were taken at times where the surface pressure was constant at increasing NG subphase concentrations from 0.28 up to 10 mM, the last concentration being higher than the cmc of NG (cmc_{NG} = 8 mM).[43]

The adsorption of NG at the air−water interface involves conformational changes of the alkyl chains, which are reflected in the antisymmetric (ν_{as}) and symmetric (ν_s) methylene stretching modes at about 2925 and 2850 cm^{-1}, respectively. Due to their conformational sensitivity, these modes can be empirically correlated with the trans/gauche ratio of the alkyl chains. Whereas the wavenumber and the bandwidth increase with an increasing number of gauche conformers, lower wavenumbers are characteristic for an ordered *all-trans* conformation of the chains.[44−46]

Figure 1A shows the intensity changes of the CH_2 antisymmetric stretching vibrational band at increasing NG concentration in the subphase (see corresponding IRRA spectra in ref 47). The absorbance increases with increasing NG concentration up to a 2.22 mM subphase concentration and continuously decreases again at higher NG concentrations (4.17, 6.11, and 8 mM). NG concentrations above the cmc show no effect on the band intensity, indicating a saturated surface at and above the cmc. As evident from Figure 1B, the frequency of the band maximum is shifted to lower wavenumber. The lowest frequency ($\nu_s(CH_2)$ = 2853 cm^{-1}) is observed at the cmc of NG (see Figure 1B). This frequency shift indicates an increase of the conformational order of the alkyl chains due to the increased surface density.

A possible explanation for the intensity decrease of the methylene stretching bands is given by Tung et al.,[48] who showed that the intensity of the CH_2 antisymmetric stretching band decreases with increasing tilt of the alkyl chains with respect to the normal of the water surface. This is due to the fact that with increasing tilt angle the transition dipole moment for the CH_2 stretching vibrations, which is oriented perpendicular to the chain axis, changes its orientation with respect to the angle of the incident light.

The increasing chain tilt angle is also reflected in the slightly stronger frequency shift at 3−5 mM NG compared to the shift seen for SDS[49] as a comparison (see Figure 1B). For SDS the alkyl chains are not tilted but change in a continuous way up to the cmc of SDS (cmc_{SDS} = 8.73 mM)[43] and therefore do not reach the low-frequency values observed for NG. The latter is due to a closer packing of the tilted alkyl chains of NG. The sugar headgroup of NG with its larger cross-sectional area prevents the alkyl chains from closer packing and forces the chains to tilt in order to realize better van der Waals contacts.

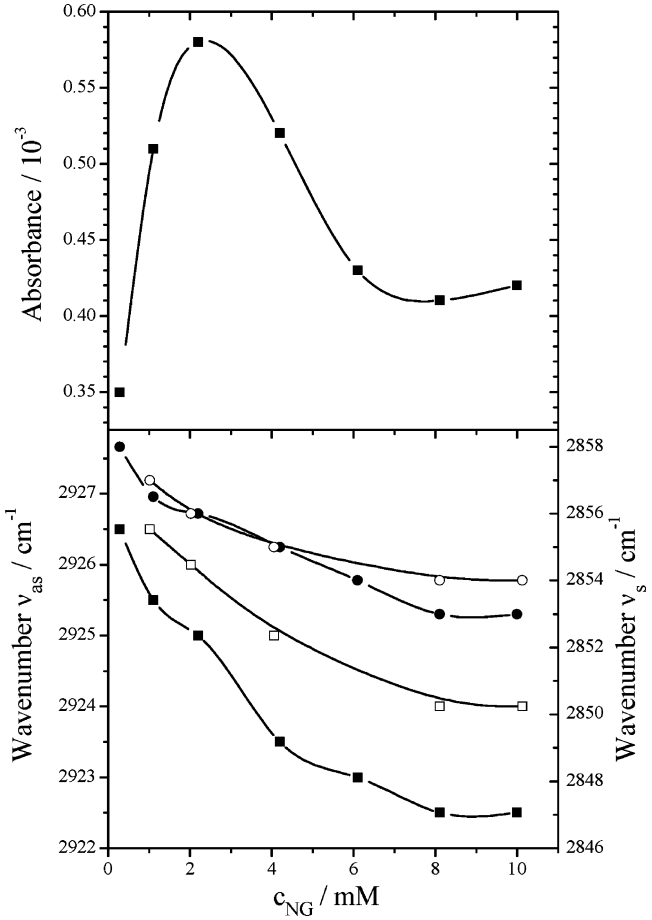

Figure 1. (A, top panel) Absorbance values of the CH_2 antisymmetric stretching vibrational band of Gibbs monolayers of NG adsorbed at the air−water interface for a series of NG subphase concentrations (points from left to right): (a) 0.28, (b) 1.1, (c) 2.2, (d) 4.2, (e) 6.1, (f) 8.1, and (g) 10 mM. (B, bottom panel) Wavenumber of the methylene stretching vibrational bands of NG at the air−water interface. Variations in wavenumber for the antisymmetric (■) and symmetric (●) stretching vibrational bands are shown as a function of NG concentration in the subphase. Experimental values for SDS are shown for comparison (open symbols).[49]

Further evidence for our assumption of tilted chains comes from the OH stretching band at 3560 cm^{-1}. Figure 2 shows the intensity changes of this band with increasing NG concentration. The absorbance value reaches a maximum at 2.22 mM of NG and decreases at higher concentrations up to a NG concentration of 8 mM. The intensity of the OH stretching band in IRRA spectra depends on the film thickness and its optical constants.[50,51] For a quantitative interpretation the latter have to be known. Then the absolute film thickness can be calculated in certain cases (Kerth, A.; Gericke, A.; Blume, A. Unpublished results). For a qualitative interpretation of our observations, we can assume that the average layer thickness of NG increases with increasing NG concentration on the surface up to a concentration of 2.22 mM and then decreases at higher concentration up to 8 mM and above the cmc. A value for the refractive index of 1.41 for the CH_2 stretching vibrational bands was used for the estimation of the layer thickness as reported by Flach et al.[52]

The assignment of IR-active vibrations from the sugar headgroup of NG is not unambiguous because of a variety of overlapping vibrational bands. The vibrations with the highest transition dipole moment are the C−O−C ring stretching and the C−O−H deformational bands between 1100 and 990 cm^{-1}, whereas the C−C vibrational bands are very weak. A fundamental vibrational analysis of β-D-glucopyranose was given by

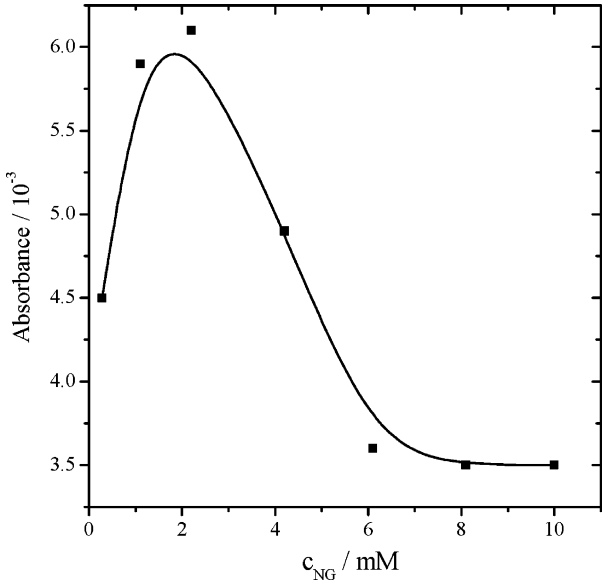

Figure 2. Absorbance values of the OH stretching vibrational band of Gibbs monolayers of NG adsorbed at the air−water interface for a series of NG subphase concentrations (points from left to right): (a) 0.28, (b) 1.1, (c) 2.2, (d) 4.2, (e) 6.1, (f) 8.1, and (g) 10 mM.

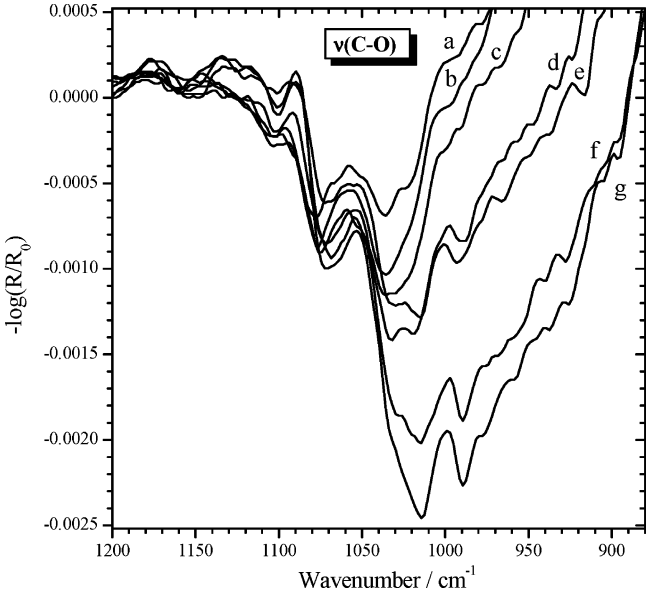

Figure 3. IRRA spectra of Gibbs monolayers of NG adsorbed at the air−water interface in the C−O stretching region for a series of NG subphase concentrations: (a) 0.28, (b) 1.1, (c) 2.2, (d) 4.2, (e) 6.1, (f) 8.1, and (g) 10 mM.

Hineno,[53] who calculated vibrational frequencies by normal coordinate treatment using the Urey−Bradly force field based on the molecular geometry of X-ray diffraction data (see Table 1). The interpretation is still complicated due to an overlap of the C−O−H deformational bands with the C−O−C and C−O−H stretching bands and the skeletal ring vibration of the sugar headgroup. Figure 3 shows IRRA spectra of the fingerprint region at increasing NG concentration up to 10 mM. The intensity of the first band at 1079 cm^{-1} increases slightly, and the maximum of the band frequency shifts to 1068 cm^{-1}. Further bands with initial frequencies of 1036, 1022, and 989 cm^{-1} show a continuous increase of their intensity up to the highest NG concentration. However, the relative intensities of the band at 1068 cm^{-1} and at 1020 cm^{-1} change, the lower frequency band increasing more strongly and becoming the prominent band at the highest concentration. In addition, its frequency decreases

TABLE 1: Observed and Calculated Frequencies and Assignments for the Sugar Headgroup Region of β-D-Glucopyranose[53] and NG

ν_{obs} [53] (cm^{-1})	ν_{calc} [53] (cm^{-1})	assignment[53]	ν_{obs}^{NG} (cm^{-1})	ν_{calc}^{NG} (cm^{-1})	assignment^{NG}
1080	1096	ν_{CO}, ν_{CC}	1068−1079	1079	ν_{COH}, ν_{CC}, δ_{COH}
1049	1070	ν_{CO}	1036	1043	ν_{COC}, ν_{COH}, δ_{COH}
1014	1014	ν_{CO}, ν_{CC}, δ_{CCO}	1014−1020	1019	ν_{COH}, δ_{COH}
	987	ν_{CC}, δ_{CCO}	990	987	ν_{COC}, ν_{CC}, δ_{COH}

to 1014 cm^{-1}. The frequency of the band at 989 cm^{-1} stays more or less constant.

Table 1 shows measured and calculated vibrational frequencies as well as the corresponding band assignments. The normal-mode analysis is based on force field simulations with the *Discover* molecular simulation program applying the COMPASS force field. Measured and calculated frequencies as well as the corresponding assignments are compared to the results of Hineno.[53] The agreement between observed and calculated wavenumbers is satisfactory. Deviations of the observed wavenumbers for β-D-glucopyranose and NG may be due to the comparison of a randomly oriented bulk system with a two-dimensional system at the air−water interface with oriented molecules. The frequency shifts observed are probably caused by changes in intermolecular interactions between the sugar groups, which are increased when the surface density is high and the molecules are tilted. In addition, changes in orientation of the headgroups can also play a role. In general, only shifts to lower frequencies are observed. For vibrational modes where OH groups are involved this could be caused by increased intermolecular hydrogen bonding, and this is to be expected when the sugar groups are in contact at a molecular area of ca. 40 $Å^2$ (see below).

For surfactant concentrations below the cmc, the surface concentrations at the interface can be estimated from the Gibbs adsorption isotherm, which in the case of uncharged surfactants and in the absence of added electrolytes is defined by eq 1:[54]

$$\Gamma = -\frac{1}{RT}\left(\frac{d\gamma}{d \ln c}\right)_T \quad (1)$$

Here Γ is the surface excess concentration, γ is the surface tension, and c is the bulk surfactant concentration. The surface tension is directly measured using the Wilhelmy technique and relates to the surface pressure π by $\gamma = \gamma_0 - \pi$, where γ is the surface tension for a monolayer-covered water surface and γ_0 the surface tension of the clean water surface ($\gamma_0 = 72$ mN/m). Figure 4 shows the Gibbs adsorption isotherm measured for the adsorption of NG at the air−water interface using the Wilhelmy plate method. It is evident from the isotherm that the surface tension decreases with increasing NG concentration, but at the cmc the surface tension stays nearly constant, which indicates that the saturation is reached.

From the adsorption isotherm the surface density of NG molecules (N) is calculated according to $N = \Gamma N_A$, which finally gives the surface area $A_s = 1/N$, needed for the construction of the π/A_s isotherm of NG (see Figure 5). At the cmc, the surface density is found to be 4.3×10^{-6} mol/m^2, which corresponds to a surface area per molecule of 38.6 $Å^2$. Reference values for alkyl glucosides from the literature vary between 38 $Å^2$ for *n*-octyl-β-D-glucopyranoside and 45 $Å^2$ for *n*-nonyl-β-D-glucopyranoside.[55−57] From these results and the wavenumbers of the methylene stretching bands, which are 2922.5 cm^{-1} for the antisymmetric and 2853 cm^{-1} for the symmetric stretching band, the alkyl chains in the NG monolayer at a subphase concentration of the cmc have to be disordered, with still a large number of gauche conformers.

Adsorption Kinetics of NG. *Surface Pressure Measurements.* Figure 6 shows the time-dependent changes in the characteristic IRRAS modes together with the surface pressure in an IRRAS contour plot. On the bottom, the surface pressure is given for the whole adsorption process, covering seven injections of small aliquots of NG stock solutions, leading to subphase concentrations of 0.28 up to 10 mM. The course of the surface pressure as a function of time after the first injection is quite unusual, as

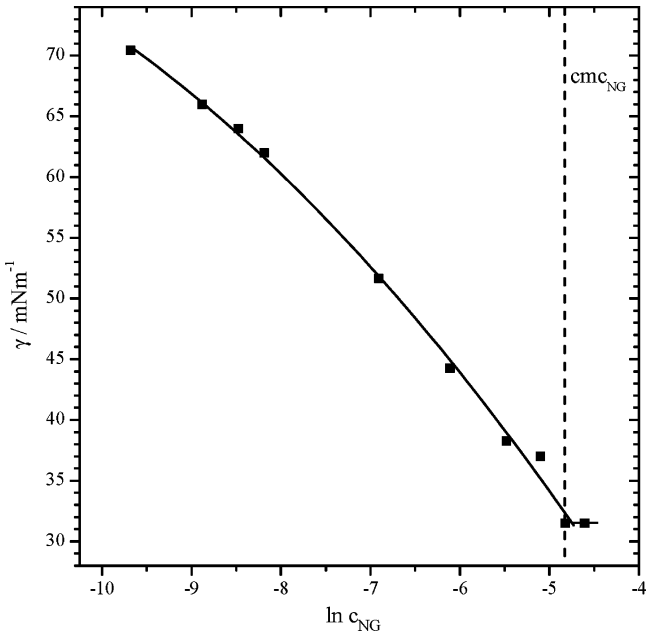

Figure 4. Dependence of the surface tension of an aqueous NG solution as a function of concentration. The cmc of NG is indicated by a vertical dotted line.

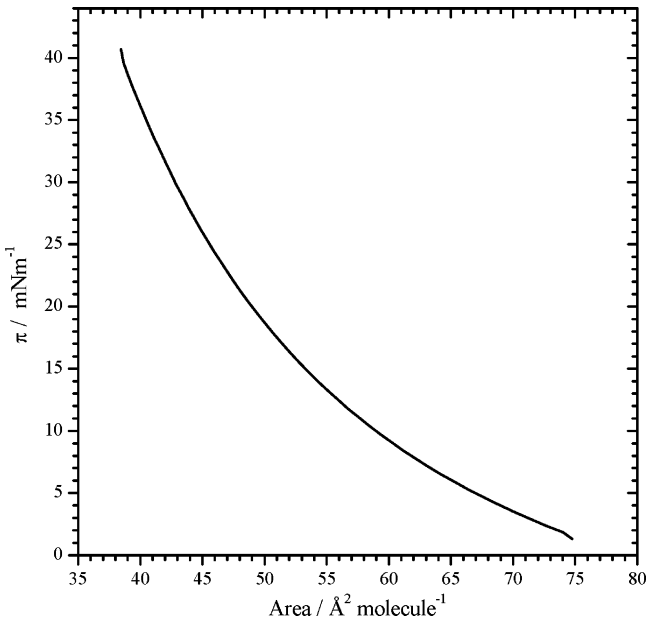

Figure 5. Calculated surface pressure/area isotherm of Gibbs monolayers of NG at the air−water interface at 293 K.

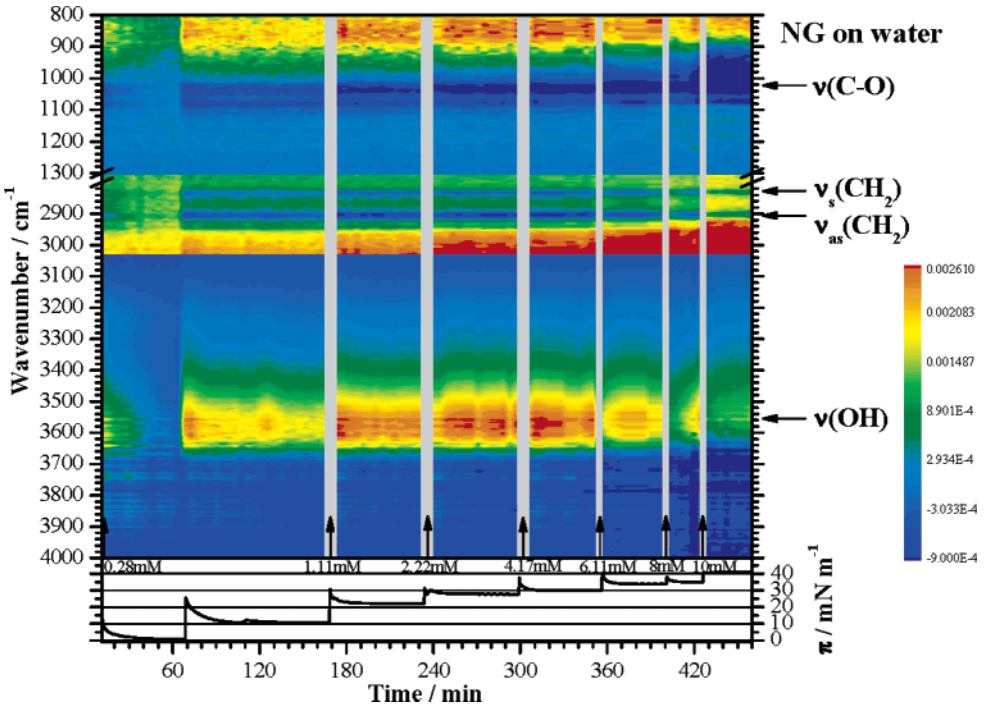

Figure 6. IRRAS contour plot of adsorbed NG at the air−water interface in the spectral regions from 4000 to 3040, from 3040 to 2800, and from 1300 to 800 cm^{-1}. The intensities are color-coded from blue (negative bands) to red (positive bands). Subphase concentrations after NG injection are indicated on the bottom by arrows, where the surface pressure is plotted versus time. IRRA spectra taken directly during the NG injections are omitted for clarity reasons (gray lines).

a sudden second surface pressure increase is observed (see at 69 min). The reason for this behavior will be discussed later. The contour plot shows the IRRA spectra, where the intensities are color-coded from blue (negative bands) to red (positive bands). The spectra are presented in a vertical direction; i.e., the wavenumber is plotted on the *Y* axis. The color codes for spectral regions of interest from 4000 to 3040, from 3040 to 2800, and from 1300 to 800 cm^{-1} were separately adjusted for better visualization of their intensity profiles. The gray lines replace the spectra taken directly during the NG injections. At this moment, the injected volume induces a sudden change in the water level of the sample trough, preventing the accumulation of spectra with good quality. The contour plot gives an overview of the spectral changes during the NG adsorption; the details, such as band frequencies and absorbance values, will be discussed separately.

As stated above, we observed an unusual change of the surface pressure during the adsorption process of NG at the air−water interface after the first injection as shown in the bottom part of Figure 6. After the first injection of NG through the air−water interface into the water subphase, the surface pressure increases within some seconds to 17.6 mN/m and decreases slowly to 0.55 mN/m within 1 h. Then, surprisingly, a second surface pressure increase to 25.5 mN/m occurs, and afterward, the surface pressure decreases until a constant value of 10.6 mN/m is reached. Assuming a diffusion coefficient of 1×10^{-9} m^2/s for a surfactant molecule, the root-mean-square displacement in 1 h can be calculated to ca. 4−5 mm. This corresponds roughly to the depth of our trough. So the observed effects are within the time expected for the diffusion of molecules in unstirred systems. As the complete mixing of the injected NG volume of 25 μL in the water subphase (14.4 mL) seems to be a diffusion-controlled process, we made analogous measurements in a different trough (11.15 mL) equipped with magnetic stirrer in order to check how additional stirring and shorter diffusion distances affect the time course of the adsorption

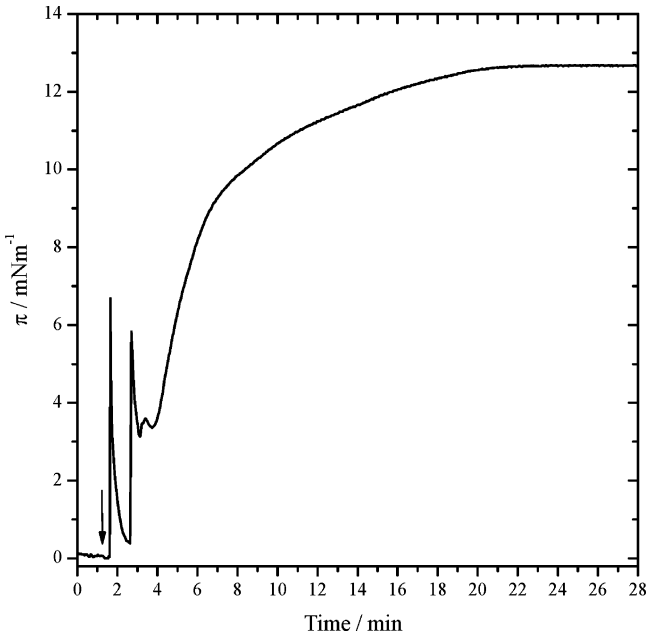

Figure 7. π as function of time after injection of 7 μL of NG (0.4 M) into the water subphase of a small round trough equipped with magnetic stirrer (final trough concentration, 250 μM). The injection is indicated by an arrow.

process. Figure 7 shows the time-dependent surface pressure during this adsorption process of NG in this small round trough under conditions of stirring. Several seconds after the injection of the NG solution, the first surface pressure increase occurs. Then, the pressure decreases to a value of 0.4 mN/m. After a delay of 60 s a second surface pressure increase occurs, and then the pressure decreases, increases again, and finally reaches a constant value of 12.5 mN/m. This result confirms the exceptional behavior of the surface pressure during the adsorption of NG observed before in the smaller IRRAS trough without

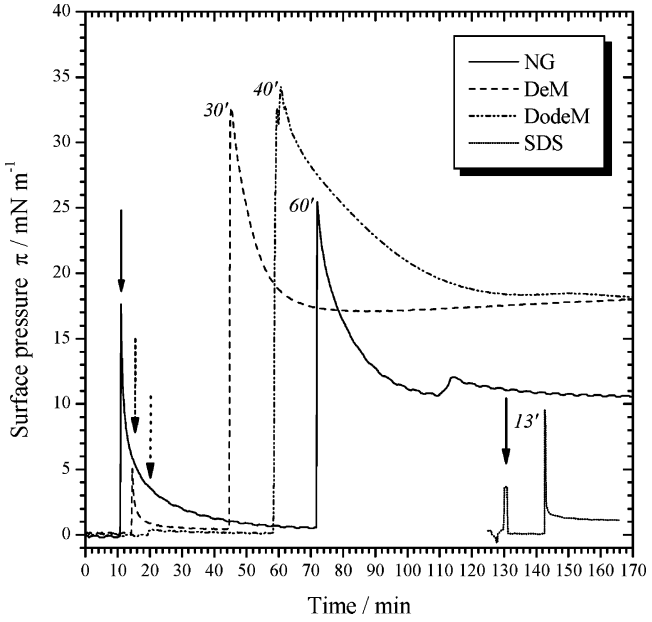

Figure 8. π as function of time after injection of 10 μL of NG (0.4 M), 18 μL of DeM (0.2 M), 9 μL of DodeM (0.04 M), and 18 μL of SDS (0.4 M) into the water subphase of the small IRRAS trough. Arrows indicate the time at which injection occurred. Numbers designate the delay time between injection and the second sharp surface pressure maximum in minutes. The curve for SDS is shifted in time for reasons of clarity.

stirring, only the kinetics is much faster due to the stirring and the smaller trough. At present, we have no satisfactory explanation for the differences observed in the small trough with stirring in comparison with the unstirred trough. The possibility that the intermediate surface micelles are different in size and number under stirring conditions cannot be ruled out. The observed different size and shape of the second surface pressure jump could then be related to these structural differences.

To clarify whether this behavior is unique for NG or typical for all surfactant molecules, we investigated the adsorption kinetics of DeM, DodeM, and SDS, which possess longer alkyl chains compared to NG and in the case of SDS also a negatively charged headgroup in the small IRRAS trough again, where the kinetics is slower. Figure 8 shows the time course of the surface pressure during the adsorption of these surfactants compared to NG. The delay time between injection and the second surface pressure maximum is different for the various surfactants. However, a direct comparison and interpretation of the adsorption kinetics is difficult, because the cmc values, the injected surfactant concentrations and volumes, and consequently the subphase concentrations are different. In all cases the subphase concentration was adjusted to a value being at least seven times lower than the cmc. As is evident from Figure 8, for all investigated surfactants two surface pressure increases are observed, suggesting a comparable time-dependent adsorption behavior at the air−water interface.

Combination of Surface Pressure and IRRAS Measurements. To explain the unusual pressure change during the adsorption of NG, IRRA measurements were performed to investigate the structural arrangement of the NG molecules at the air−water interface. The shuttle technique limits the time resolution of IRRA measurements to one spectrum within 4 min. However the temporal resolution is high enough to follow spectral changes during the drastic surface pressure changes. Figure 9 shows IRRA spectra of the OH and CH_2 stretching region at the first metastable pressure plateau just before and just after the second pressure increase. The enormous difference

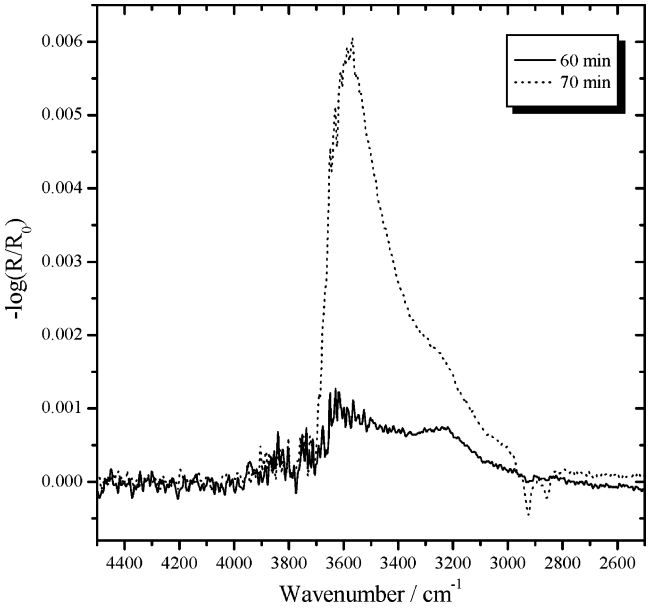

Figure 9. IRRA spectra of Gibbs monolayers of NG adsorbed at the air−water interface in the OH and CH_2 stretching region after different adsorption times: (a) 60 and (b) 70 min.

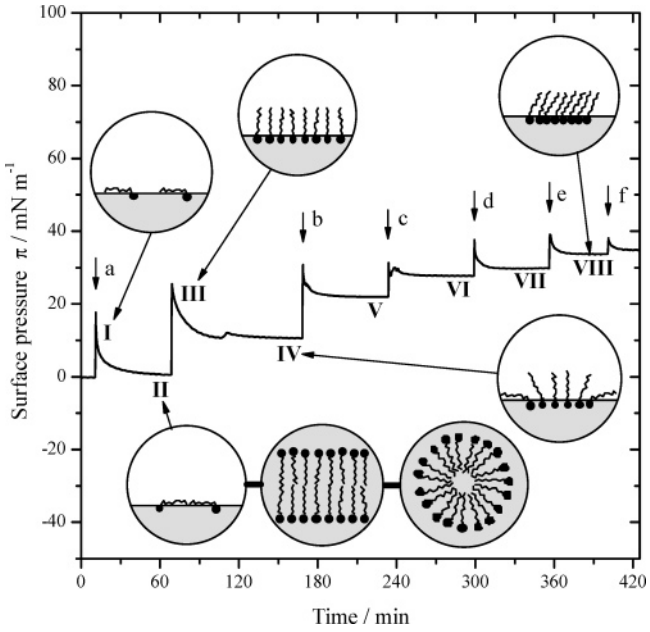

Figure 10. Proposed arrangement of NG molecules (I−VIII) during the adsorption process at the air−water interface at different subphase concentrations and surface pressures: (a) 0.28, (b) 1.11, (c) 2.22, (d) 4.17, (e) 6.11, (f) 8, and (g) 10 mM.

of the OH band intensity indicates a large difference in the film thickness before and after the pressure increase, suggesting a complete rearrangement of the NG molecules. The difference in the CH_2 stretching band intensity confirms this assumption. We believe that this sudden jump in pressure is not due to a sudden adsorption process but is caused by a change in the orientation and arrangement of the surfactant molecules already present an the air−water interface. Taking into consideration all available information, namely, the change in the surface pressure as well as the intensities of the CH_2 and OH stretching bands, we are now able to discuss possible structural changes during the adsorption process of NG at the air−water interface. Figure 10 shows the proposed different arrangements of NG molecules during the adsorption process at the air−water interface at different surface pressures. Selected points (I−VIII)

TABLE 2: NG Subphase Concentrations, Surface Pressures, and Absorbance Values of the Antisymmetric CH_2 and OH Stretching Bands for Selected Points (I−VIII) in the π/Time Curve (See Figure 10) of the NG Adsorption Process at the Air−Water Interface

	c (10^{-3} M)	π (mN m^{-1})	A_{CH_2} (10^{-3})	A_{OH} (10^{-3})
I	0.28	11.1		
II	0.28	0.5	0.08	1
III	0.28	25.5	0.55	6
IV	0.28	10	0.36	4.5
V	1.11	21.9	0.51	6
VI	2.22	27.8	0.58	6.2
VII	4.17	33.7	0.52	4.9
VIII	6.11	35	0.43	3.5

in the π/time curve are described in Table 2 by means of the NG subphase concentration, the surface pressure, and the absorbance of the antisymmetric CH_2 and OH stretching bands.

After the first injection of NG at the bottom of the small IRRAS trough, the immediate pressure increase to 11.1 mN/m indicates that a certain number of NG molecules are present at the air−water interface at the beginning, caused by the introduction and the removal of the syringe with attached minute amounts of surfactant solution on the needle. The IR band intensities observed during this time period are omitted in Table 2 (point I), because this process depends on the specific injection procedure. After the injection the surface pressure decreases to 0.5 mN/m due to the fact that NG molecules introduced into the air−water interface are partitioned into the subphase whereas NG molecules injected into the trough below the air−water surface have not yet had time enough to arrive at the interface by diffusion. Furthermore, NG molecules possibly aggregate at the interface, also leading to a decrease of the surface pressure. The reason for this aggregation may be similar to that in the bulk, namely, the gain in free energy when the hydrophobic groups are removed from contacts with water. The surface aggregation properties then depend on the structural properties of the surfactant, such as intermolecular hydrogen bonds between the sugar headgroups, hydrophobic effects, and van der Waals interactions between the alkyl chains.[11] Structural models for these so-called surface micelles were described by Israelachvili,[34] who proposed disk- and ribbonlike micelles, depending on the 2D packing parameter of the surfactant.

IRRA spectra in point II (see Figure 9 and Table 2) show extremely low intensities of the CH_2 and OH stretching bands, suggesting an unusual arrangement of the molecules. According to reports from the literature,[39,58] we assume at point II an arrangement of NG molecules parallel to the water surface (see Figure 10). A support for this assumption comes from the low intensity of the OH band ($A_{OH} = 1 \times 10^{-3}$). As mentioned above the intensity of the OH stretching band in IRRA spectra shows a correlation with the optical constants and the film thickness. In our case only a qualitative analysis of the OH stretching band is feasible, because of the additional absorption from the OH groups of the NG headgroup. Since the contribution of four OH groups per molecule cannot be neglected, the film thickness can only be estimated qualitatively, but we are sure that the film thickness decreases.

Further indications for a parallel arrangement of the NG molecules to the water surface come from the extremely low absorbance value of 0.08×10^{-3} for the antisymmetric CH_2 stretching band. A decreasing intensity of this band is directly related to an increasing tilt of the alkyl chains with respect to the normal of the water surface.[48] With increasing tilt angle, the transition dipole moment, being oriented perpendicular to the chain axis, changes its orientation with respect to the incident light. This leads to the change in absorbance intensity, which can be calculated using the Fresnel equations.[59] For an alkyl chain with all-trans conformation the intensity decreases roughly by a factor of 4 when the chains change their orientation from perpendicular to parallel to the surface. We therefore propose that, at point II, when the surface pressure is low, the surface is covered mainly with surface micelles besides some monomers. Further adsorption of surfactant molecules from the subphase would then just increase the number of surface micelles; the pressure would stay almost the same.

At point III we observe a sudden increase in surface pressure to 25.5 mN/m as well as an increase in OH and CH_2 band intensities. Obviously, further NG molecules reaching the interface by diffusion from the subphase perturb the parallel arrangement of the alkyl chains in the surface micelles and induce a spontaneous rearrangement of the NG molecules to a perpendicular orientation with a concomitant dissociation of the surface micelles into monomers (see Figure 9 and Table 2, point III). The OH band intensity corresponds to a value typical for amphiphiles with alkyl chains oriented perpendicular to the water surface, having in mind that the OH groups from the sugar headgroup contribute to the OH band intensity. With time the surface pressure decreases to 10 mN/m, which may now be due to an aggregation of NG molecules in the perpendicular orientation caused by intermolecular hydrogen bonds between the sugar headgroups and van der Waals interactions of the alkyl chains. At the same time, the film thickness and the CH_2 band intensity decrease slightly, indicating a possible disordering of the alkyl chains.

After point IV, the second injection takes place and increases the subphase concentration to 1.11 mM. We observe just a small pressure peak, and then the surface pressure stays constant at 21.9 mN/m. Further injections lead to a situation where each injection increases the surface pressure but the OH and CH_2 band intensities are decreasing. This can be interpreted as being caused by a tilt of the now more ordered alkyl chains, as the lower frequency of the antisymmetric stretching band (2923 cm^{-1}) compared to point IV (2926.5 cm^{-1}) indicates.

The kinetic model for the adsorption of NG at the air−water surface is at present very preliminary. One could suggest that at low packing densities the averaging of the motions of the disordered chains is around the surface normal and all orientations are equally probable in the average chain orientation. When the surface density is increased, hydrogen bond interactions between the sugar headgroups come into play and the sugar residues are hindered in their reorientational motions. Because the chains have a certain orientation with respect to the plane of the sugar headgroup, the reorientational motions of the chains are now around a tilted axis and not around the surface normal. This would imply a local biaxiality. Macroscopically, however, this would not be observable due to the dynamics of the system and the smallness of the domains.

The adsorption kinetics of SDS at low subphase concentration shows a comparable behavior of the molecules at the air−water interface. This can be deduced from the differences in the OH and CH_2 band intensities before and after the second pressure increase (not shown). Obviously, the presence of functional groups, which can be linked by hydrogen bonds as in the case of NG is not a prerequisite for this type of micellar aggregation at the air−water interface.

Summary and Conclusions

The two-dimensional self-assembly of amphiphilic molecules at the air−water interface may induce the formation of "surface

micelles", which are too small to be observed directly with current experimental techniques. Our spectroscopic observations during the adsorption of NG using IRRAS in connection with the surface pressure/time behavior support the notion that these aggregates are intermediate structures during the adsorption of surfactants at the air−water interface. Applying the IRRAS technique, we studied in detail the adsorption kinetics of the surfactant NG at the air−water interface after injection of the surfactant into the subphase. The adsorption kinetics was followed by changes in the surface pressure and of the intensity of the CH_2 bands of the chains and of the OH vibrational band, which is directly related to the layer thickness. During an induction period, when the molecules are still highly diluted, they aggregate to surface micelles with their chains oriented parallel to the air−water interface and the surface pressure is low. After some time when more molecules reach the surface from the subphase, they suddenly rearrange to an upright orientation and the surface micelles dissociate. A further increase in subphase concentration then only increases the number of molecules at the air−water interface, the molecules become more tightly packed, and the chains are more ordered and start to tilt at higher surface coverage. The observations are discussed in comparison to results obtained for the adsorption kinetics of DeM, DodeM, and SDS.

Acknowledgment. This work was supported by grants from the Deutsche Forschungsgemeinschaft and the Fonds der Chemischen Industrie. Accelrys Inc. is acknowledged for providing us with the COMPASS force field.

Note Added after ASAP Publication. On the seventh page of this paper, right column, second line, the reference cited after "Fresnel equations" has been corrected. This paper was originally posted ASAP on 3/5/2005. The corrected version was posted on 3/9/2005.

References and Notes

(1) Monteux, C.; Williams, C. E.; Meunier, J.; Anthony, O.; Bergeron, V. *Langmuir* **2004**, *20*, 57−63.
(2) Harada, M.; Okada, T. *Langmuir* **2004**, *20*, 30−32.
(3) Ignés-Mullol, J.; Claret, J.; Sagués, F. *J. Phys. Chem. B* **2004**, *108*, 612−619.
(4) Kent, M. S.; Yim, H.; Sasaki, D. Y. *Langmuir* **2004**, *20*, 2819−2829.
(5) He, Q.; Zhai, X.; Li, J. *J. Phys. Chem. B* **2004**, *108*, 473−476.
(6) Grigoriev, D.; Miller, R.; Wüstneck, R.; Wüstneck, N.; Pison, U.; Möhwald, H. *J. Phys. Chem.* **2003**, *107*, 14283−14288.
(7) Malec, A. D.; Wu, D. G.; Louie, M.; Skolimowski, J. J.; Majda, M. *Langmuir* **2004**, *20*, 1305−1310.
(8) Penfold, J.; Sivia, D. S.; Staples, E.; Tucker, I.; Thomas, R. K. *Langmuir* **2004**, *20*, 2265−2269.
(9) Vollhardt, D.; Fainerman, V. B. *J. Phys. Chem. B* **2004**, *108*, 297−302.
(10) Nandi, N.; Vollhardt, D.; Brezesinski, G. *J. Phys. Chem. B* **2004**, *108*, 327−335.
(11) Prosser, A. J.; Retter, U.; Lunkenheimer, K. *Langmuir* **2004**, *20*, 2720−2725.
(12) Ward, A. F. H.; Tordai, L. *J. Chem. Phys.* **1946**, *14*, 453.
(13) Chang, Ch.-H.; Franses, E. I. *Colloids Surf.* **1995**, *100*, 1.
(14) Goncalves da Silva, A. M.; Guerreiro, J. C.; Rodrigues, N. G.; Rodrigues, O. T. *Langmuir* **1996**, *12*, 4442−4448.
(15) Dudnik, V.; Lunkenheimer, K. *Langmuir* **2000**, *16*, 2802−2807.
(16) Dynarowicz, P.; Paluch, M. *J. Colloid Interface Sci.* **1989**, *129*, 379−383.
(17) Retter, U. *Langmuir* **2000**, *16*, 7752−7756.
(18) Gilchrist, V. A.; Lu, J. R.; Garrett, P.; Penfold, J. *Langmuir* **1999**, *15*, 250−258.
(19) Meunier, J. *Colloids Surf. A* **2000**, *171*, 33−40.
(20) Lösche, M.; Möhwald, H. *Rev. Sci. Instrum.* **1984**, *55*, 1968−1972.
(21) Möller, G.; Schradre, S.; Motschmann, H.; Prescher, D. *Langmuir* **2000**, *16*, 4594−4598.
(22) Bell, G. R.; Li, Z. X.; Bain, C. D.; Fischer, P.; Duffy, D. C. *J. Phys. Chem. B* **1998**, *102*, 9461−9472.
(23) Kambhampati, D. K.; Knoll, W. *Curr. Opin. Colloid Interface Sci.* **1999**, *4*, 273−280.
(24) Vollhardt, D.; Fainerman, V. B. *Adv. Colloid Interface Sci.* **2000**, *86*, 103−151.
(25) Als-Nielsen, J.; Jacquemain, D.; Kjaer, K.; Leveiller, F.; Lahav, M.; Leiserowitz, L. *Phys. Rep.* **1994**, *246*, 251−313.
(26) Beattie, D. A.; Haydock, S.; Bain, C. A. *Vib. Spectrosc.* **2000**, *24*, 109−123.
(27) Dluhy, R. A.; Cornell, D. G. *J. Phys. Chem.* **1985**, *89*, 3195−3197.
(28) Albrecht, O.; Gruler, H.; Sackmann, E. *J. Phys. (Paris)* **1978**, *39*, 301−313.
(29) Yue, B. Y.; Jackson, C. M.; Taylor, J. A. G.; Mingins, J.; Pethica, B. A. *J. Chem. Soc., Faraday Trans. 1* **1982**, *78*, 323−339.
(30) Miller, A.; Möhwald, H. *J. Chem. Phys.* **1987**, *86*, 4258−4265.
(31) (a) Flörsheimer, M.; Möhwald, H. *Colloids Surf.* **1991**, *55*, 173−189. (b) Buffeteau, T.; Blaudez, D.; Pere, E.; Desbat, B. *J. Phys. Chem. B* **1999**, *103*, 5020−5027.
(32) Chi, L. F.; Anders, M.; Fuchs, H.; Johnston, R. R.; Ringsdorf, H. *Science* **1993**, *259*, 213−216.
(33) Sankaram, M. B.; Marsh, D.; Thompson, T. E. *Biophys. J.* **1992**, *63*, 340−349.
(34) Israelachvili, J. *Langmuir* **1994**, *10*, 3774−3781.
(35) Ren, Y.; Iimura, K.-I.; Ogawa, A.; Kato, T. *J. Phys. Chem. B* **2001**, *105*, 4305−4312.
(36) Ren, Y.; Iimura, K.-I.; Kato, T. *J. Phys. Chem. B* **2002**, *106*, 1327−1333.
(37) Maaloum, M.; Muller, P.; Krafft, M. P. *Angew. Chem.* **2002**, *114*, 4507−4510.
(38) Lunkenheimer, K.; Earnshaw, J. C.; Barzyk, W.; Dudnik, V. *Prog. Colloid Polym. Sci.* **2000**, *116*, 95−99.
(39) Lunkenheimer, K.; Barzyk, W.; Hirte, R.; Rudert, R. *Langmuir* **2003**, *19*, 6140−6150.
(40) Ward, A. F. H.; Tordai, L. *J. Chem. Phys.* **1946**, *14*, 453−461.
(41) Fainerman, V. B.; Miller, R. *J. Colloid Interface Sci.* **1996**, *178*, 168−175.
(42) Flach, C. R.; Brauner, J. W.; Taylor, J. W.; Baldwin, R. C.; Mendelsohn, R. *Biophys. J.* **1994**, *67*, 402−410.
(43) Majhi, P. R.; Blume, A. *Langmuir* **2001**, *17*, 3844−3851.
(44) Snyder, R. G.; Aljibury, A. L.; Strauss, H. L.; Casal, H. L.; Gough, K. M.; Murphy, W. F. *J. Chem. Phys.* **1984**, *81*, 5352−6361.
(45) Snyder, R. G.; Strauss, H. L.; Elliger, C. A. *J. Phys. Chem.* **1982**, *86*, 5145−5150.
(46) Snyder, R. G.; Hsu, S. L.; Krimm, S. *Spectrochim. Acta, Part A* **1978**, *34*, 395−406.
(47) Meister, A.; Kerth, A.; Blume, A. *Phys. Chem. Chem. Phys.*, in press.
(48) Tung, Y.-S.; Gao, T.; Rosen, M. J.; Valentini, J. E.; Fina, L. J. *Appl. Spectrosc.* **1993**, *10*, 1643−1650.
(49) Meister, A.; Kerth, A.; Blume, A. *J. Phys. Chem. B* **2004**, *108*, 8371−8378.
(50) Kerth, A. Ph.D. Dissertation, MLU Halle-Wittenberg, Germany, 2003.
(51) Hussain, H.; Kerth, A.; Blume, A.; Kressler, J. *J. Phys. Chem. B* **2004**, *108*, 9962−9969.
(52) Flach, C. R.; Gericke, A.; Mendelsohn, R. *J. Phys. Chem. B* **1997**, *101*, 58−65.
(53) Hineno, M. *Carbohydr. Res.* **1977**, *56*, 219−227.
(54) Hiemenz, P. C.; Rajagopalan, R. In *Principles of Colloid and Surface Chemistry*; Marcel Dekker Inc.: New York, 1997; p 327.
(55) Kjellin, U. R. M.; Claesson, P. M.; Vulfson, E. N. *Langmuir* **2001**, *17*, 1941−1949.
(56) Rosen, M. J.; Sulthana, S. B. *J. Colloid Interface Sci.* **2001**, *239*, 528−534.
(57) Ericsson, C. A.; Söderman, O.; Garamus, V. M.; Bergström, M.; Ulvenlund, S. *Langmuir* **2004**, *20*, 1401−1408.
(58) Fainerman, V. B.; Makiewski, A. V.; Joos, P. *Colloids Surf. A* **1994**, *90*, 213−224.
(59) Mendelsohn, R.; Brauner, J. W.; Gericke, A. *Annu. Rev. Phys. Chem.* **1995**, *46*, 305−334.